Lab on a Chip

A membrane-based immunosensor enabling high antifouling performance and sensitive molecular recognition

Journal:	*Lab on a Chip*
Manuscript ID	LC-ART-01-2025-000031.R1
Article Type:	Paper
Date Submitted by the Author:	06-Apr-2025
Complete List of Authors:	Yamashita, Hiroki; Institute of Science Tokyo Institute of Integrated Research Laboratory for Chemistry and Life Science Okuyama, Hiroto ; Institute of Science Tokyo Institute of Innovative Research, Laboratory for Chemistry and Life Science Yamaguchi, Takeo; Institute of Science Tokyo Institute of Integrated Research Laboratory for Chemistry and Life Science

PAPER

A membrane-based immunosensor enabling high antifouling performance and sensitive molecular recognition

Received 00th January 20xx,
Accepted 00th January 20xx

DOI: 10.1039/x0xx00000x

Hiroki Yamashita, Hiroto Okuyama and Takeo Yamaguchi*

The fouling of non-targeted biomolecules on sensing surfaces, which can cause a reduction in sensing performance, is a severe problem in immunosensing platforms. The incorporation of hydrophilic polymers on sensing surfaces is effective against antifouling. However, such an approach can reduce the density of the capture antibody, resulting in a decrease in sensitivity and signal output. Here, both high sensitivity and antifouling properties were achieved using a porous-membrane-based immunosensor. This sensor can drastically mitigate the signal reduction due to the introduction of an antifouling moiety by antibody densification in submicron-scaled pores. The ideal ratio of the receptor/antifouling moiety was estimated from numerical modeling. The high sensitivity and antifouling properties of the designed sensor were demonstrated via the detection test of interleukin-6 (IL-6). The proposed sensor exhibited excellent antifouling and high sensitivity with limits of detection of 4.8 and 1.2 pg/mL in artificial saliva and serum, respectively. The study findings highlight the potential of membrane-based sensors for practical diagnoses.

Introduction

The demand for rapid diagnoses performed at home or by the bedside, called point-of-care testing (POCT), is increasing because of various factors, such as the aging population, shortage of doctors, and global spread of infectious diseases in developed countries.[1–3] In this context, the immunosensor is a promising POCT device that functions based on antigen–antibody reactions. In the design of immunosensors, high sensitivity is required to accurately determine the level of disease and/or the necessity for additional medical treatments. To achieve high sensitivity, several approaches for signal amplification have been demonstrated, including promotive antigen–antibody reactivity through microchannels,[4–7] electrochemical signal amplification,[8–11] and target labeling by enzymes,[12,13] nanoparticles,[14–17] and functional polymers.[18–21] In addition, it is crucial to achieve a low background in biological samples. The background can increase through the nonspecific adsorption of biomolecules onto the sensing interface, and this can severely affect the sensitivity and reliability of the test results. In the enzyme-linked immunosorbent assay (ELISA), which is known as the “gold standard” of immunoassays, a blocking agent is typically used to cover the adsorptive sites. However, this method can cause an undesirable covering of the reactive surface, which results in low sensitivity.[22] Sample dilution is another simple method; however, it also causes the dilution of target molecules. The introduction of hydrophilic antifouling polymers on sensing surfaces is a promising approach to inhibiting fouling.[23–25] Zwitterionic polymers can form a strong hydration layer on material surfaces and increase the osmotic pressure against the insertion of biomolecules.[26] However, conventional biosensors suffer from a trade-off between molecular recognition ability and antifouling properties. An increase in the amount of the antifouling moiety can cause a decrease in the immobilized antibody, resulting in low sensitivity (**Error! Reference source not found.**a).[27–29]

Previously, we developed a membrane-based immunosensor that uses the submicron-scaled pores of track-etched porous membranes for molecular recognition.[30] This sensor achieved a high signal output through the accumulation of the capture antibody in the pores. In addition, rapid detection was achieved through analyte permeation through the pores, promoting molecular recognition. The sensor functioned as a microfluidic sensor with numerous submicron channels. The potential of this sensor was demonstrated via the detection of the inflammatory marker interleukin-6 (IL-6) in a model buffer, and a limit of detection (LOD) of 4.5 pg/mL was obtained.[31] This sensor should be endowed with antifouling properties to inhibit fouling in practical diagnoses using biological samples, such as serum and saliva. The pores have a large surface area per space and can maintain high antibody density while introducing antifouling polymers. Thus, the potential to achieve both antifouling properties and high sensitivity exists.

Here, we developed a membrane-based immunosensor that enables both antifouling properties and high signal characteristics under complex analyte conditions (**Error!**

Laboratory for Chemistry and Life Science, Institute of Integrated Research, Institute of Science Tokyo, Yokohama, Kanagawa 226-8501, Japan. E-mail: yamag@res.titech.ac.jp

† Electronic supplementary information (ESI) available. See DOI: 10.1039/x0xx00000x

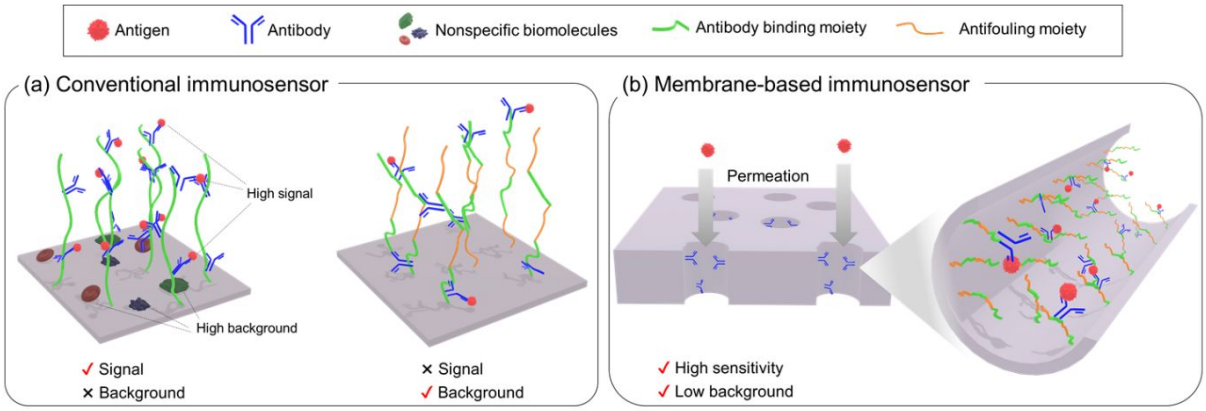

Reference source not found.b).

Fig. 1 Comparison of (a) conventional and (b) membrane-based immunosensors. The decrease in recognizability associated with the introduction of antifouling moieties is resolved in membrane-based sensors using a small pore space and solution permeation.

First, the correlation between the composition of the density of the capture antibody and the sensing performance in the membrane-based sensor and conventional ELISA was estimated via a numerical modeling. The model suggested that there was room to introduce an antifouling moiety while maximizing the signal output only in the case of a membrane-based sensor. We experimentally developed the IL-6 immunosensor; the sensing performance of the sensor was investigated in artificial saliva and serum to demonstrate its potential for POCT devices.

Methods

Materials and reagents

A track-etched polyethylene terephthalate (PET) membrane substrate (porosity = 17.3%, pore density = 2.2×10^7 cm^{-2}, pore diameter = 1 µm, thickness = 22 µm. The information was provided by manufacturer) with cylindrical pores was purchased from it4ip (Louvain-la-Neuve, Belgium). A porous PE membrane substrate (porosity = 50.0%, average pore diameter = 200 nm, thickness = 25 µm) was supplied by Asahi-Kasei (Tokyo, Japan). Furthermore, 2-methacryloyloxyethyl phosphorylcholine (MPC), sodium dodecyl sulfate (SDS), (1R,8S,9s)-bicyclo[6.1.0]non-4-yn9-ylmethyl N-succinimidyl carbonate (BCN-NHS), tris(hydroxymethyl)aminomethane, Tween 20, and ascorbic acid were purchased from TCI (Tokyo, Japan). Glycidyl methacrylate (GMA), sodium azide (NaN_3), ammonium chloride (NH_4Cl), 1 M sulfuric acid (H_2SO_4); *N,N*-dimethylformamide (DMF); disodium hydrogen phosphate (Na_2HPO_4); potassium chloride (KCl); sodium chloride (NaCl); calcium chloride ($CaCl_2$); urea; mucin; human serum albumin (HSA); sodium hydrogen carbonate ($NaHCO_3$); glucose; fructose; uric acid; L-cysteine; and magnesium sulfate ($MgSO_4$) were purchased from FUJIFILM Wako Pure Chemical Corporation (Osaka, Japan). In addition, 3,3′,5,5′-tetramethylbenzidine (TMB) solution and fluorescein isothiocyanate (FITC)-labeled anti-BSA antibody were purchased from Bethyl Laboratories. MN Sterilizer cellulose acetate (CA; pore size = 0.2 µm) was purchased from MACHEREY-NAGEL GmbH & Co. KG (Düren, Germany). Human IL-6 antibody (capture antibody), recombinant human IL-6 protein (antigen), human IL-6 biotinylated antibody (detection antibody), and horseradish peroxidase (HRP)-labeled streptavidin were purchased from R&D systems (Minneapolis, Minnesota, USA). FITC-labeled BSA was purchased from Thermo Fisher Scientific (Waltham, Massachusetts, USA). Phosphate-buffered salt (PBS: 10 mM, pH = 7.4) tablets were purchased from Takara Bio (Shiga, Japan). PBS and Tris-buffered saline with Tween 20 (TBST: 50 mM tris(hydroxymethyl)aminomethane, 138 mM NaCl, 2.7 mM KCl, 0.05% w/v Tween 20, pH = 8.0) were prepared using Milli-Q water. Artificial saliva was prepared by dissolving 0.6 g/L Na_2HPO_4, 0.6 g/L $CaCl_2$, 0.4 g/L KCl, 0.4 g/L NaCl, 4 g/L mucin, and 4 g/L urea in Milli-Q water and adjusted to a pH of 7.2 through the addition of NaOH. Artificial serum was prepared by dissolving 1% (w/v) HSA, 150 mM NaCl, 18 mM $NaHCO_3$, 5.55 mM glucose, 4.3 mM urea, 0.4 mM fructose, 0.4 mM uric acid, 0.055 mM ascorbic acid, 0.1 mM L-cysteine, and 0.87 mM $MgSO_4$ in a 100 mM phosphate buffer and adjusted to a pH of 7.4 through the addition of NaOH.

Numerical modeling of the amount of sandwich complex between the membrane-based immunosensor and ELISA

In the modeling of ELISA and the membrane-based immunosensor, the amount of the sandwich complex (capture antibody–antigen-detection antibody) was calculated and compared at varying densities of the capture antibody (σ_{Ab}). In both models, the recognition condition at each step was unified as (1) antigen at concentrations C_{Ag} in the range of 1–1000 pg/mL for 10 min and (2) detection antibody at a concentration of 200 ng/mL for 30 min. It was assumed that the same sample volume as ELISA (100 µL) was used to compare the amount of the sandwich complex. Table S1 lists the parameters used in the calculations.

In the ELISA model, the σ_{Ab} (ng/cm^2) was defined as the immobilized antibody per well surface area (6 mm, diameter; 3.5 mm, height). The active σ_{Ab} was assumed to be 5% of the maximum adsorption density of the antibody on a standard polystyrene plate.[32] The antigen–antibody reaction is assumed to only occur by diffusion on the well surface. COMSOL

Multiphysics was employed to simulate biomolecular diffusion and calculate the amount of the sandwich complex on the well surface. In the membrane-based sensor, the σ_{Ab} was defined as the immobilized antibody per total surface area, including the membrane pores. Here, the analyte solution was assumed to permeate through the cylindrical pores with a diameter of 1 μm. The model of the membrane-based immunosensor has been previously constructed and details are shown in supporting information.[32] Briefly, the model does not include fitting parameters but comprises an advective term with the Lax–Wendroff theorem, which is a nonlinear equation with second-order accuracy in space and time, and a reaction term for the antigen–antibody reaction in the pore (**Error! Reference source not found.**). For instance, the step for antigen recognition can be described as follows:

$$\frac{\partial C_{\mathrm{Ag}}}{\partial t} = -\vec{u}\frac{\partial C_{\mathrm{Ag}}}{\partial x} - k_{\mathrm{on}}C_{\mathrm{Ag}}C_{\mathrm{Ab}} + k_{\mathrm{off}}C_{\mathrm{Ab-Ag}} \quad (1)$$

Here, k_{on} and k_{off} are the association and dissociation rate constants, respectively, in the recognition of antigen, u is the flow rate of the analyte, $C$is the concentration of each biomolecule. It is important to note that the total pore surface area is significantly larger than the external membrane surface area (by more than tenfold); therefore, the model considers only antigen recognition occurring within the pores. In addition, the model can simulate the experimental results without considering the radial distribution of biomolecules, as the kinetics of antigen diffusion in the radial direction are sufficiently fast compared to the kinetics of antigen recognition and flow velocity.[32]

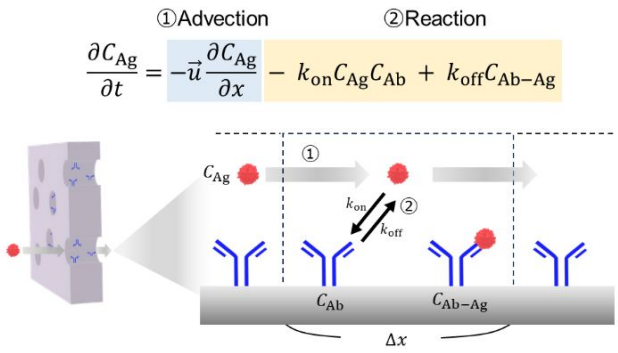

Fig. 2 Schematic illustration of the molecular recognition system in the membrane pore. The model is based on the advection term and reaction term.

Plasma-induced graft polymerization

Scheme 1 shows a schematic representation of the membrane-based immunosensor. In this study, GMA was used as a monomer for antibody introduction, and MPC was used as an antifouling moiety to suppress fouling. PolyGMA (PGMA) was grafted onto PET membranes via plasma-induced graft polymerization (PIGP), according to our previous report.[31] Poly (MPC-*co*-GMA) ($PMPC_x$-GMA_y)-grafted membranes were prepared using the aforementioned method (x and y represent the molar ratio). The pristine PET membrane was cut into 3 × 3 cm^2 and rinsed using water and ethanol. Thereafter, the membrane was placed in a glass ampoule and treated with argon plasma for 1 min at a pressure of 10 Pa and a power of 30 W. The plasma-treated membrane was exposed to air for 1 min to generate peroxide groups on its pores and external membrane surface.[33] The membrane was immersed in an aqueous solution of 5 wt% monomers with 10 wt% SDS. The membrane-immersed solution was degassed by N_2 bubbling for 10 min and set in a water bath shaker (MM-10, TAITEC) at 80°C for 30 min to initiate graft polymerization.[34,35] After the polymerization, the membrane was washed overnight with a 50% aqueous ethanol solution and dried under vacuum at 50°C for 4 h. To confirm the graft polymerization, the weight change of the membrane prior to and after graft polymerization was measured. The grafting ratio of the membrane φ [%] was calculated as follows:

$$\varphi\,[\%] = \frac{W_{\mathrm{graft}} - W_{\mathrm{sub}}}{W_{\mathrm{sub}}} \times \frac{1-\alpha}{\alpha} \times 100 \quad (2)$$

where W_{sub} (g) and W_{graft} (g) are the dry weight of the membrane prior to and after the PIGP, respectively. α (-) is the membrane porosity.

The composition of the grafted polymer was investigated using a PE membrane. The PIGP were applied to the PE membranes, and Fourier transform infrared (FTIR) spectra were recorded using an FTIR spectrometer (FT/IR-6200, JASCO Corp.) to determine the exact ratio of MPC and GMA in the grafted polymers.

Introduction of reactive group into membrane pores and immobilization of capture antibody in membrane

The experiments were conducted as previously described.[31] Briefly, six millimoles of NaN_3 and NH_4Cl each were dissolved in DMF (20 mL). The membranes obtained after PIGP were immersed in the aforementioned solution, and the azidation of the epoxy group in GMA was performed for 2 h at 60°C. The membranes were rinsed with a 50% aqueous ethanol solution. Afterward, the membranes were immersed in 1 M H_2SO_4 overnight at 30°C for the remaining epoxy groups to react. In each step, the membranes were analyzed via FTIR. The hydrophilicity of the prepared PET/$PMPC_x$-GMA_y membranes was evaluated through water contact angle measurements (Drop Shape Analyzer, DSA100, KRÜSS). Azide/diol-modified membranes were cut into circles (diameter = 1 cm), and each membrane was placed in a 24-well microplate. Subsequently, the solution of the capture antibody modified with cyclooctyne (250 μg/mL, 100 μL) was dropped onto the membrane. The membranes were incubated for 48 h at 20°C. After incubation, the membranes were rinsed with pure water and used in IL-6 detection tests.

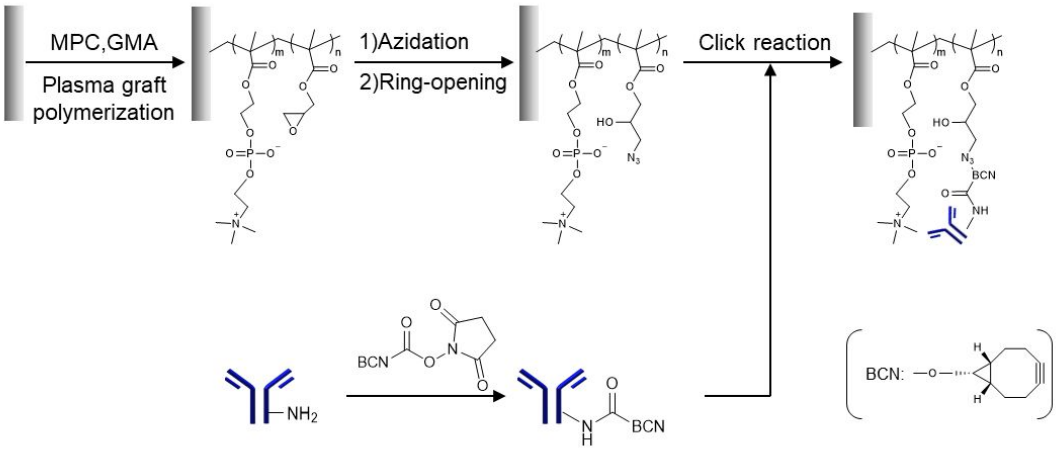

Scheme 1 Schematic representation of the fabrication of membrane-based immunosensor.

Characterization of the membrane-based immunosensor

The composition ratio of the graft copolymers was determined by FTIR analysis. The MPC content was calculated from the peak area of the phosphorylcholine group (1000–1330 cm^{-1}), and the GMA content was calculated from the peak area of the carbonyl group (1670–1780 cm^{-1}), after subtracting the overlapping contribution from MPC. Immobilization of the antibody and fluorescence imaging were conducted as previously reported.[31] Briefly, FITC-labeled antibody was immobilized on the membrane according to the described protocol. The membranes were then sectioned, and cross-sectional images were obtained using confocal laser scanning microscopy (Zeiss LSM 780). Antibody density was calculated based on the average fluorescence intensity over a defined cross-sectional area, with measurements taken from three different locations. A detailed protocol for the quantification of antibody density is provided in the Supporting Information.

IL-6 detection test in model buffer and complex solutions

An IL-6 buffer solution was prepared by dissolving IL-6 in TBST at various concentrations. IL-6 detection was performed using a membrane-based immunosensor with an anti-IL-6 capture antibody. Typical detection protocol comprised the permeation of the (1) antigen for 10 min, (2) biotinylated detection antibody for 30 min, (3) HRP-labeled streptavidin for 10 min, and (4) substrate (TMB) for 10 min. The final colored TMB solution was measured via ultraviolet–visible spectroscopy (HITACHI, UH3900D). The absorbance at 650 nm with IL-6 was defined as the signal, and the absorbance at 650 nm without IL-6 (0 pg/mL of the antigen) was defined as the background.

Artificial saliva and serum were used as models of biological analytes without dilution. Following our typical protocol, artificial saliva was used after filtration through a 0.2-µm membrane filter (CA, MACHEREY-NAGEL GmbH & Co. KG) to remove non-targeted substances, such as large mucins, as a pretreatment. A diagnostic test without pretreatment was conducted using artificial saliva as is.

Results and discussion

Numerical modeling of the amount of sandwich complex in ELISA and the membrane-based immunosensor

The feasibility of combining excellent signal output and antifouling property in a membrane-based sensor was initially demonstrated through numerical modeling. Here, the benefit of our system is also emphasized by comparing both membrane-based sensor and conventional ELISA under the same testing conditions. The adopted conditions (i.e., antigen recognition for 10 min and sandwich formation for 30 min) are the conditions we used in the previous report for IL-6 sensing, [31] and their short testing time meets the requirements of POCT. **Error! Reference source not found.**shows the estimated amount of the sandwich complex for ELISA and the membrane-based immunosensor at an IL-6 concentration of 100 pg/mL. Here, the amount of the sandwich complex was directly related to the signal intensity. In the ELISA, the amount of the sandwich complex gradually increased depending on the antibody density. However, the membrane-based sensor exhibited a significantly higher amount of the sandwich complex compared with ELISA, and it maximized at an antibody density of 50 ng/cm². Similar trends in the sandwich complex were observed at varying IL-6 concentrations (Figure S1). These trends were derived from the difference in reactivity in the antigen recognition step. In this step, the kinetics of antigen recognition can be expressed as $v = kC_{Ag}C_{Ab}$, where C_{Ag} and C_{Ab} are the concentrations of the antigen and capture antibody, respectively. In the case of the ELISA, v was proportional to C_{Ab} when σ_{Ab} is small and C_{Ag} could be considered constant. Oppositely, in the high σ_{Ab} region, the concentration gradient of the antigen was observed, and the slow diffusivity of the antigen limited the reactivity (in other words, the kinetics was dominated by antigen diffusion). Consequently, the amount of the sandwich complex in the ELISA was modestly correlated with the antibody density; however, it was limited even at a high σ_{Ab}. The antigen reactivity (ratio of the captured antigen to the

total antigen) estimated from the modeling was only 22% at σ_{Ab} = 600 ng/cm². Contrarily, the membrane-based sensor overcame this limitation through the convective flow and antibody accumulation in submicron-scaled pores. In other words, reactions in the small pore spaces eliminate the influence of antigen diffusion. Thus, the membrane-based sensor enabled ~100% of antigen reactivity within the region of σ_{Ab} > 50 ng/cm².

This suggests that the membrane-based sensor can achieve both sensitivity and antifouling properties, which is difficult in conventional immunosensors. Based on the experimental investigations, the σ_{Ab} of the reported membrane-based sensor without antifouling moieties was 170 ng/cm². This was sufficiently larger than that of the required antibody density (σ_{Ab} > 50 ng/cm²), thus, there is a room to replace the antibody with an antifouling moiety.

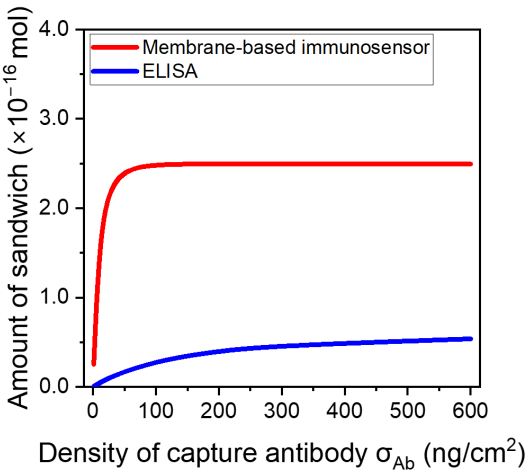

Fig. 3 Estimated amount of sandwich complex in the IL-6 detection of 100 pg/mL in an ELISA and using the membrane-based immunosensor via numerical modeling.

Fabrication and characterization of membrane-based immunosensor with antifouling properties

We experimentally demonstrated the proposed sensor with high sensitivity and antifouling properties. The polymer grafting in the membrane pores was confirmed by weight change and FTIR spectroscopy. The grafting ratio determined from the weight change was 6.5 ± 1.5%, which was controlled to provide sufficient reaction sites without a reduction in permeability. The composition of the grafted polymer was calculated from the FTIR spectra. However, when a PET membrane was used as the substrate, large and complex peaks originating from ester and phenyl groups hindered the quantification of the MPC and GMA signals. Therefore, a porous PE membrane was alternatively used in the FTIR analysis. The validity of this approach was also demonstrated in our previous report.[31]

Error! Reference source not found.a shows the FTIR peaks after the PIGP, azidation, and ring-opening reaction. After grafting the MPC and GMA copolymers, peaks of phosphate groups derived from MPC (1080 and 1240 cm^{-1}), epoxy groups derived from GMA (900 cm^{-1}), and carbonyl groups derived from MPC and GMA (1730 cm^{-1}) were observed. After the azidation, the peak at 900 cm^{-1} decreased, and the peak of the azide group was observed at 2100 cm^{-1}, indicating that the epoxy group had been converted into the azide group. In this step, the composition ratio of the graft copolymers could be controlled by the feed ratio of the monomers (**Error! Reference source not found.**). **Error! Reference source not found.**b shows the results of the water contact angle measurements on the PET/$PMPC_x$-GMA_y membranes. As expected, the contact angle decreased with an increase in the MPC ratio.

To verify antibody immobilization in the membrane pores, the FITC-labeled anti-BSA antibody was immobilized on the membrane, and the fluorescence intensity in the membrane pore was analyzed via fluorescence microscopy. At low MPC ratios (**Error! Reference source not found.**a, b), significant fluorescence was observed along the straight pore structure, confirming the uniform immobilization of the FITC-labeled antibodies. At high MPC ratios (**Error! Reference source not found.**c–e), the uniform immobilization of the antibodies was also confirmed; however, the fluorescence intensity was inversely correlated with the MPC ratio (**Error! Reference source not found.**f). The amount of azide groups in the pore was stoichiometrically excessive for antibody immobilization even at an MPC ratio of 87%. Thus, the decrease in the introduced antibody may have been derived from a decrease in the reactivity of the click reaction. The Fc region of the antibody that includes the click reactive site is hydrophobic; thus, the access of the antibodies to the reaction site in the grafted polymers was probably inhibited by an increase in the MPC proportion. Consequently, depending on the MPC ratio in the grafted polymer, the antibody density in the pore was controlled within the range of 1–170 ng/cm². Based on the modeling results in Figure 2b, the MPC ratio should be x < 40% to obtain a maximized signal.

In our sensor, the cost of antibody represents the major portion of the overall design expense, thus, reducing the quantity of antibody is crucial matter. The ratio of immobilized antibody to the amount prepared was inversely correlated with the MPC content in the grafted polymer. As shown in Table S2, the immobilization efficiency ranged from 0.1% to 9.0%. These results suggest that further optimization of the reaction conditions and/or immobilization system could reduce antibody usage, especially in sensors containing MPC.

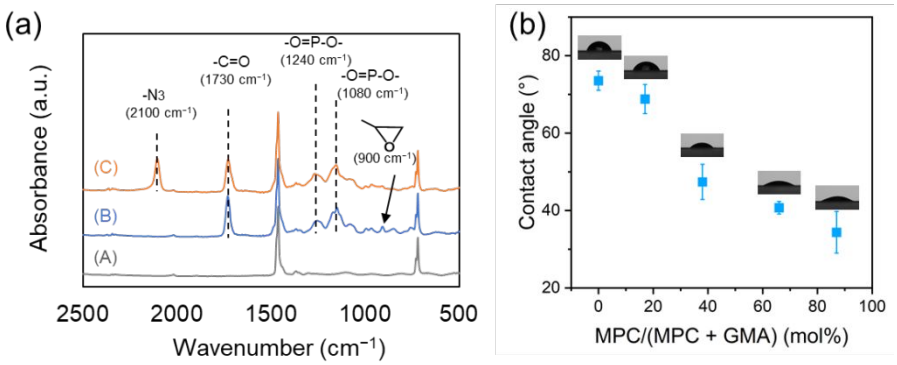

Fig. 4 (a) FTIR spectra of the membranes prior to and after the reaction step of (A) the PE substrate, (B) after copolymer grafting, and (C) after the azidation and ring-opening reactions. The peaks are representative results using PE/PMPC$_{17}$-GMA$_{83}$. (b) Water contact angle of membranes after the grafting of the PMPC$_x$-GMA$_y$ copolymer.

Table 1 Relationship between the composition of the reaction solution and the monomer ratio in the copolymer.

Monomer ratio in feed [mol%]		Monomer ratio in copolymer [mol%]		Abbreviation
MPC	GMA	MPC	GMA	
0	100	0	100	PET/PGMA
50	50	17	83	PET/PMPC$_{17}$-GMA$_{83}$
70	30	38	62	PET/PMPC$_{38}$-GMA$_{62}$
80	20	66	34	PET/PMPC$_{66}$-GMA$_{34}$
90	10	87	13	PET/PMPC$_{87}$-GMA$_{13}$

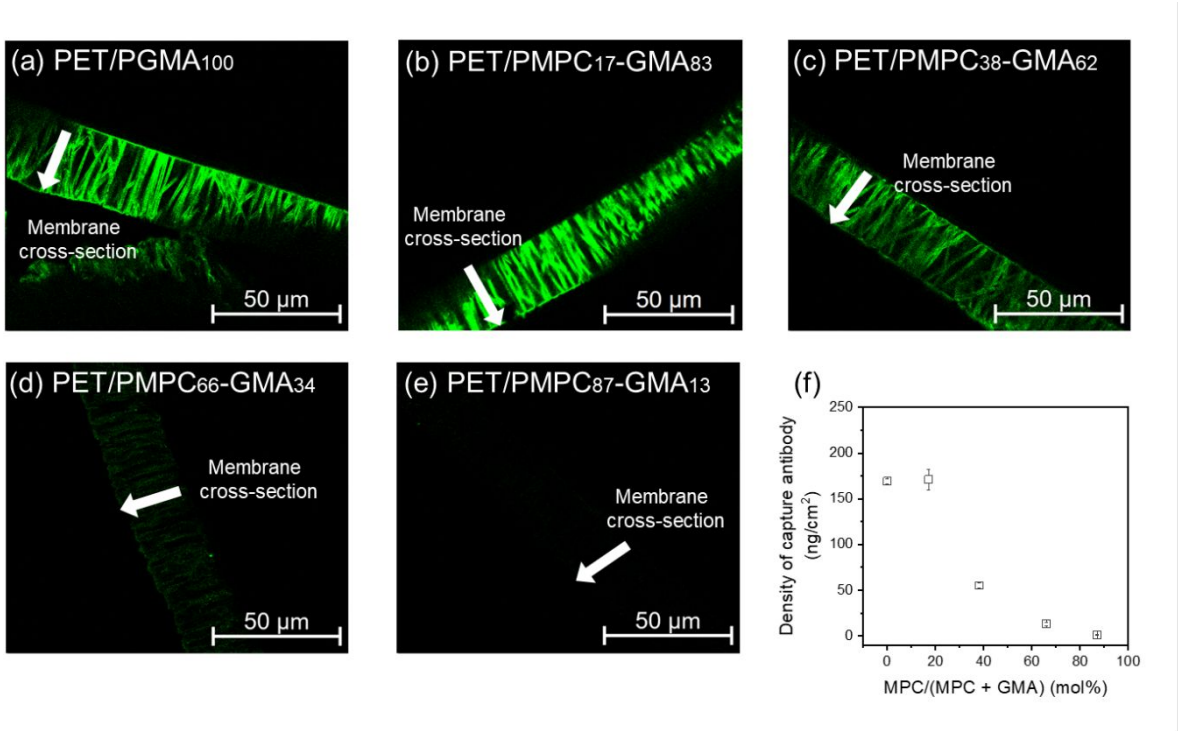

Fig. 5 (a–e) Cross-sectional fluorescent images of the membrane after FITC-labeled antibody immobilization. (f) The density of capture antibody at different MPC ratios. The density of the capture antibody was calculated from the fluorescence intensity based on a report (the calculation is described in the Supporting Information).

Evaluation of membrane-based sensor performances via IL-6 detection in buffer solution

The relationship between the antibody density in the membrane pore and the signal characteristics was investigated through immunosensing tests using sensors fabricated with different copolymer compositions. The cytokine IL-6 was used as a biomarker for the sensing test. IL-6 is an inflammation biomarker and is used in the diagnosis of various diseases, such as coronavirus disease 2019, cancer, Alzheimer's disease, depression, and sepsis. Thus, the monitoring of IL-6 levels plays an important role in determining disease levels.[38] **Error! Reference source not found.** shows the relationship between the obtained signal and the density of the capture antibody during the sensing test of 100 pg/mL IL-6 in TBST. The result shows that the performance was consistent with the predictions in our modeling; the signal intensity was maximized at the MPC ratio of $x < 40\%$.

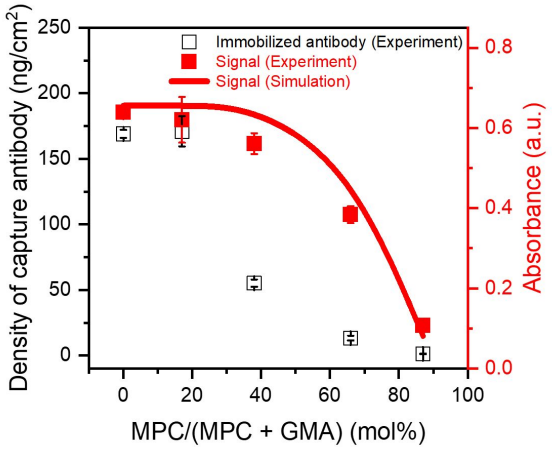

Fig. 6 Density of capture antibody at different MPC ratios, and comparison of experimental and calculated signals (IL-6, 100 pg/mL) by numerical modeling.

Evaluation of membrane-based sensor via IL-6 detection in biomimetic analytes

The IL-6 levels in saliva and serum are the pg/mL ranges observed under healthy conditions but can exceed 100 pg/mL depending on pathological levels.[36] Thus, the sensitivity of the pg/mL level in complex biological samples is required for IL-6 sensors. Here, IL-6 detection tests were conducted using artificial saliva and serum samples as model complex analytes to demonstrate sensitive sensing in complex samples. Using artificial saliva (**Error! Reference source not found.**a), the signal output was maximized for the sensor with an MPC ratio below 40%, and it decreased beyond 40% MPC, exhibiting a trend similar to that observed in the IL-6 detection in a buffer (**Error! Reference source not found.**). However, in the sensor without an MPC moiety, the background in artificial saliva was comparable to the signal (**Error! Reference source not found.**b). This may have been due to the adsorption of nonspecific substances in the artificial saliva onto the reactive sites and its interaction with the detection antibody. This result correlates with that of the protein adsorption test using the FITC-BSA shown in Figure S2, where the degree of fouling on PET/PGMA considerably exceeded that on the MPC-introduced membrane. The background of the MPC-introduced sensor was significantly low (<0.05) at the MPC ratio of $x > 17\%$; thus, the selective detection of IL-6 was achieved under these conditions. This value was relatively smaller than the reported values required to effectively exhibit antifouling properties. For instance, Akkahat et al. designed a biosensing platform utilizing MPC-contained copolymer brushes and reported excellent antifouling properties with 79% MPC.[29] Similarly, Wiarachai et al. emphasized the importance of increasing the MPC units for effective antifouling in biosensors; their platform achieved superior antifouling properties and sensing capabilities at an MPC ratio of 55%.[37] The present sensor exhibited an effective antifouling performance at a lower MPC ratio probably because of the flow-based sensing system. In such immunoassays, the flow effectively removes nonspecific residues on the sensor surface, thereby reducing background signals and improving sensitivity.[38]

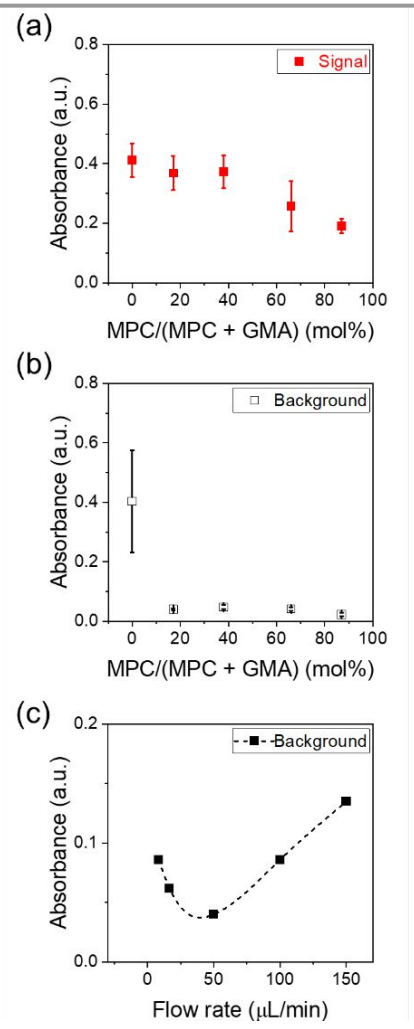

Fig. 7 (a) Signal of IL-6 (100 pg/mL) and (b) background signal in artificial saliva at different MPC ratios in the graft polymer. (c) Background signal in artificial saliva at different flow rates during the first step of IL-6 detection.

We further investigated the correlation between analyte flow rate (J, µL/min) and background signal. As shown in Fig. 7c, the background was minimized at 50 µL/min, which was also adopted as the standard condition in our sensing protocol. The reduction in background at $0 < J < 50$ is attributed to the removal of nonspecific residues via solution flow. In contrast, the increase in background at $J > 50$ is likely due to partial collapse of the hydration layer on the grafted polymer under high shear stress.[39]

The sensing performance was further investigated using the PET/PMPC$_{17}$-GMA$_{83}$ sensor. **Error! Reference source not found.**a and b show the calibration curve for IL-6 detection in artificial saliva. The LOD of the sensor was 4.8 pg/mL based on the 3SD/slope. The linearity of the sensor was dependent on the concentration of IL-6, and the sensing range was 4.8–300 pg/mL. IL-6 detection was conducted in artificial serum. An excellent sensitivity with an LOD of 1.2 pg/mL and a high linearity in the range of 1.2–300 pg/mL (**Error! Reference source not found.**c, d) were observed. These values fulfill the sensitivity requirements for several diseases. Contrarily, the PET/PGMA sensor exhibited a high background due to insufficient antifouling (Figure S3), and the calibration curve did not reveal concentration dependence (Figure S4). Thus, the designed membrane-based sensor with MPC demonstrated its capability for the selective and highly sensitive detection of IL-6 at the pg/mL level in complex analytes.

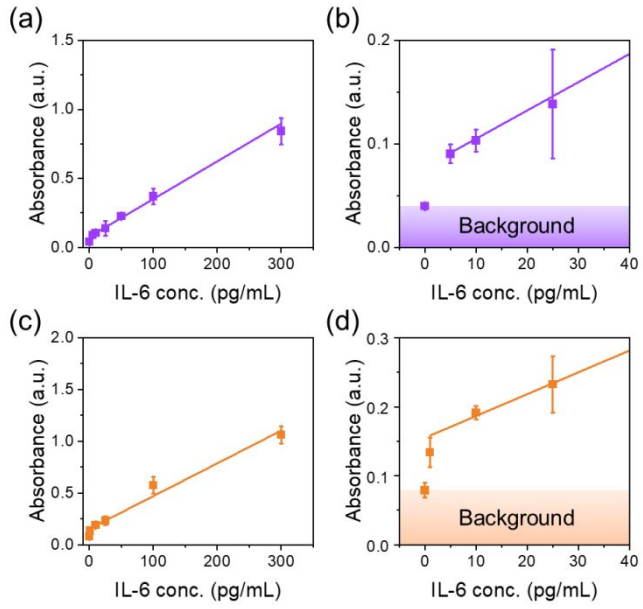

Fig. 8 (a) Calibration plots for IL-6 detection in artificial saliva. (b) Enlarged linear portion at the concentrations of the antigen (0–40 pg/mL) in (a). (c) Calibration plots for IL-6 detection in artificial serum. (d) Enlarged linear portion at the concentrations of the antigen (0–40 pg/mL) in (c). The sensing tests depicted in (a)–(d) were conducted using the PET/PMPC17-GMA83 sensors. The calibration line displayed in (c) and (d) is the same as that in (a) and (b).

IL-6 detection test in artificial saliva without pretreatment

In a typical immunoassay, additional pre-operation may be required depending on the analyte, which is undesirable for POCT. For instance, in the case of saliva, dilution or centrifugation is frequently required before diagnosis because mucin (high molecular weight glycoprotein that causes high viscosity) and/or food residues degrade sensor performance. For membrane-based sensors, macromolecules can lead to pore blockage and the degradation of the sensing ability because the sensor uses submicron-scaled small pores for the recognition space. This challenge can be resolved without additional steps and an increase in testing time by incorporating a pre-filtering mechanism into the sensing system. Here, we attempted to validate a sensing system that simultaneously performs pretreatment and molecular detection by connecting the prefilter and membrane-based sensor (PET/MPC$_{17}$-GMA$_{83}$) in series (**Error! Reference source not found.**a). During this test, the IL-6 detection in artificial saliva was conducted within the range of 0–300 pg/mL of IL-6. **Error! Reference source not found.**b, c shows the high linear relationship, low background, and selective detection of IL-6 with a significant signal comparable to the results of the sensing test using buffer solutions. Thus, the proposed sensor can be directly used from saliva samples without any pretreatment, showing its potential as a POCT device.

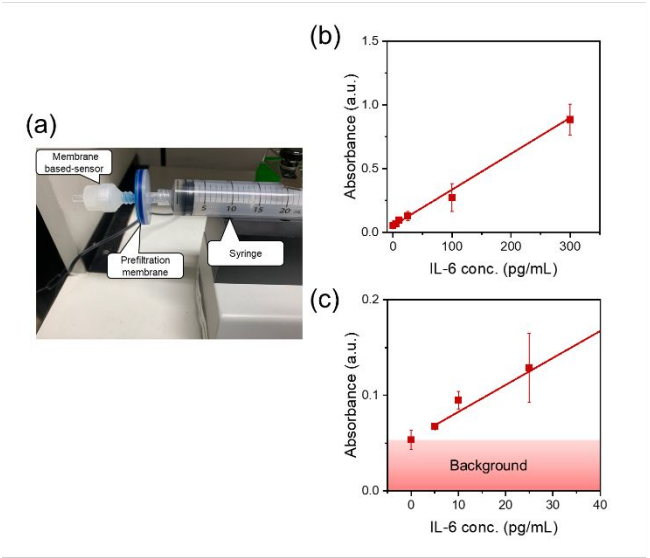

Fig. 9 (a) Equipment for membrane-based immunosensing with pre-filtration membrane. (b) Calibration plot for IL-6 sensing in artificial saliva through the system incorporating pre-filtration and sensing. (c) Enlarged linear portion at the concentrations of the antigen (0–40 pg/mL) in (b).

Conclusions

Here, we developed a membrane-based immunosensor that enables high sensitivity and antifouling properties. Numerical modeling revealed differences in the molecular recognition capabilities of conventional ELISA and membrane biosensors: slow antigen access to the well surface limits sensitivity during an ELISA. Conversely, solution flow into the pores maximizes the sensing ability at a relatively low antibody density in the membrane-based sensor. Thus, the membrane-based sensor can maintain a high detection signal with low antibody density. This was experimentally confirmed through the detection of IL-6 as a model biomarker. In the IL-6 detection test in artificial saliva and serum, the sensor with MPC drastically reduced the background and exhibited excellent antifouling properties. The proposed sensing system demonstrated excellent antifouling properties at an MPC concentration of 17%, with LODs of 4.8 and 1.2 pg/mL in artificial saliva and serum, respectively. The high performance of the proposed sensor can be maintained in complex samples by incorporating a pre-filtering membrane. It is expected that the optimal combination of a pre-filtration membrane and sensor will enable highly sensitive antigen detection without requiring sample pretreatment. Furthermore, such advanced sensing designs have the potential to improve sensor durability and extend operational lifespan in practical applications. This is one of the few studies that have integrated numerical modeling and experimental approaches in the design of immunosensors. The proposed membrane-based immunosensor holds promise as an alternative to existing sensors, including microfluidic devices.

Author contributions

Hiroki Yamashita: conceptualization, methodology, data curation, formal analysis, validation, investigation, and writing original draft; Hiroto Okuyama: writing original draft, supervision, and methodology; Takeo Yamaguchi: project administration, supervision, conceptualization, and resources.

Conflicts of interest

There are no conflicts to declare.

Data availability

The modelling and experimental data supporting this article have been included in the article and the ESI.

Acknowledgements

This work was supported by JST SPRING, Japan Grant Number JPMJSP2106 and JPMJSP2180.

References

1 J. F. Hernández-Rodríguez, D. Rojas and A. Escarpa, *Anal. Chem*., 2021, 93, 167−183.
2 L. C. Brazaca, I. Sampaio, V. Zucolotto and B. C. Janegitz, *Talanta*, 2020, 210, 120644.
3 A. A. Patil, P. Kaushik, R. D. Jain and P. P. Dandekar, *ACS Infect. Dis*., 2023, 9, 9−22.
4 X. Zhou and B. Zheng, *Lab Chip*, 2023, 23, 1151–1168.
5 E. Eteshola and D. Leckband, *Sens. Actuators B - Chem*, 2001, 72, 129–133.
6 V. Pinto, P. Sousa, S. O. Catarino, M. Correia-Neves and G. Minas, *Biosens. Bioelectron*., 2017, 90, 308–313.
7 J. Li and P. B. Lillehoj, *ACS Sens*., 2021, 6, 1270–1278.
8 J. Wang, *Electroanalysis*, 2005, 17, 7–14.
9 W. J. Shen, Y. Zhuo, Y. Q. Chai, Z. H. Yang, J. Han and R. Yuan, *ACS Appl. Mater. Interfaces*., 2015, 7, 4127–4134.
10 J. Li, H. Yang, R. Cai and W. Tan, *ACS Appl. Mater. Interfaces*., 2022, 14, 44222–44227.
11 D. Han, K. Yang, S. Sun and J. Wen, *Chem. Eng. J*., 2023, 476, 146688.
12 S. I. Funano, M. Sugahara, T. G. Henares, K. Sueyoshi, T. Endo and H. Hisamoto, *Analyst*, 2015, 140, 1459–1465.
13 Z. Gao, L. Hou, M. Xu and D. Tang, *Sci. Rep*., 2014, 4, 3966.
14 Y. Gao, Y. Zhou and R. Chandrawati, *ACS Appl. Nano Mater*., 2020, 3, 1–21.
15 W. Zhou, X. Gao, D. Liu and X. Chen, *Chem. Rev*., 2015, 115, 10575–10636.
16 Q. Zhao, D. Lu, G. Zhang, D. Zhang and X. Shi, *Talanta*, 2021, 223, 121722.
17 P. D. Howes, R. Chandrawati and M. M. Stevens, *Science*, 2014, 346.
18 S. Kim and H. D. Sikes, *Polym. Chem*., 2020, 11, 1424–1444.
19 Q. Wang, S. Yu, L. Zhang, L. Wang, J. Kong, L. Li and X. Zhang, *Chem. Commun*., 2022, 58, 1701–1703.
20 D. Cheng, Z. Zhou, S. Shang, H. Wang, H. Guan, H. Yang and Y. Liu, *Anal. Chim. Acta*, 2022, 1219, 340032.
21 C. Zhang, D. Zhang, Z. Ma and H. Han, *Biosens. Bioelectron*., 2019, 137, 1–7.
22 S. Sakaki, Y. Iwasaki, N. Nakabayashi and K. Ishihara, *Polym J*., 2000, 32, 637–641.
23 J. Baggerman, M. M. J. Smulders and H. Zuilhof, *Langmuir*, 2019, 35, 1072–1084.
24 J. T. Heggestad, C. M. Fontes, D. Y. Joh, A. M. Hucknall and A. Chilkoti, *Adv. Mater*., 2020, 32, 1903285.
25 M. J. Russo, M. Han, P. E. Desroches, C. S. Manasa, J. Dennaoui, A. F. Quigley, R. M. I. Kapsa, S. E. Moulton, R. M. Guijt, G. W. Greene and S. M. Silva, *ACS Sens*., 2021, 6, 1482–1507.
26 M. He, K. Gao, L. Zhou, Z. Jiao, M. Wu, J. Cao, X. You, Z. Cai, Y. Su and Z. Jiang, *Acta Biomater*., 2016, 40, 142–152.
27 R. Iwata, R. Satoh, Y. Iwasaki and K. Akiyoshi, *Colloids Surf. B Biointerfaces*, 2008, 62, 288–298.
28 K. Nishizawa, T. Konno, M. Takai and K. Ishihara, *Biomacromolecules*, 2008, 9, 403–407.
29 P. Akkahat, S. Kiatkamjornwong, S. I. Yusa and V. P. Hoven, *Langmuir*, 2012, 28, 5872–5881.
30 H. Okuyama, Y. Oshiba and T. Yamaguchi, *Anal. Chem*., 2019, 91, 14178–14182.
31 H. Okuyama, Y. Kodama, K. Takemura, H. Yamashita, Y. Oshiba and T. Yamaguchi, *Anal. Methods*, 2023, 15, 1494–1499.
32 H. Okuyama, T. Tamaki, Y. Oshiba, H. Ueda and T. Yamaguchi, Anal. Chem., 2021, 93, 7210–7219.

33 T. Yamaguchi, S. I. Nakao and S. Kimura, J. Polym. Sci., Polym. Chem. Ed., 1996, 34, 1203–1208
34 T. Yamaguchi, S. I. Nakao and S. Kimura, Macromolecules, 1991, 24, 5522–5527.
35 H. Okuyama, Y. Oshiba, H. Ohashi and T. Yamaguchi, *Small*, 2018, 14, 1702267.
36 L. E. McCrae, W.-T. Ting and M. M. R. Howlader, *Biosensors and Bioelectronics: X*, 2023, 13, 100288.
37 O. Wiarachai, T. Vilaivan, Y. Iwasaki and V. P. Hoven, *Langmuir*, 2016, 32, 1184–1194.
38 J. H. Cho, M. H. Kim, R. S. Mok, J. W. Jeon, G. S. Lim, C. Y. Chai and S. H. Paek, *J. Chromatogr. B*, 2014, 967, 139–146.
39 A. Belanger, A. Decarmine, S. Jiang, K. Cook and K. A. Amoako, *Langmuir*, 2018, 35, 1984–1988.

Data Availability Statement

The modelling and experimental data supporting this article have been included in the article and the ESI.